Resource assessment and site selection for solar heating and cooling systems

2

D.S. Renné
Dave Renné Renewables, LLC, Boulder, CO, United States

2.1 Introduction

The solar resource available to solar conversion technologies is highly variable, both in time and in location. This chapter focuses on how we can obtain the best possible knowledge about this variability so that solar systems can be deployed in the optimal sites and in the most efficient configurations. Notwithstanding the nocturnal and seasonal planetary cycles that affect the solar resource reaching the top of the atmosphere, weather patterns, landform characteristics, such as coastlines, and topography all play key roles in affecting the short-term variability of the resource at the earth's surface. Although knowledge of spatial variability is important for identifying preferred sites for solar systems, it is more common that a solar system will need to be sited close to a load center for optimal system efficiency. In these cases, the knowledge of spatial variability will help determine the actual resource at a specific site, even if no measurements are available for that site, and even if the site is not at the location of the highest resource.

For certain types of solar heating systems, especially those that have some form of storage capacity, the short-term weather-related variability may have only a minor impact on system design and performance. However, for large-scale solar systems, especially those that have an impact on the load profile that must be met by the electrical grid, resource variability may have significant importance, if not for the system itself, then for the utility that must serve the net load resulting from both resource variability and electrical demand.

A clear understanding of resource characteristics is important for designing the most appropriate system for a given environment and the load requirements. Because actual ground-based measurements are often lacking at most proposed sites for solar heating and cooling systems, various tools and techniques need to be brought into play to best characterize the resource so that investment risk in the project is minimized.

Fig. 2.1 outlines the basic stages that take place in a large-scale solar project and indicates what type of solar resource information is most appropriate for each stage. In this chapter, we address the basic solar principles, including definitions, measured and modeled solar radiation data, and adaptation of solar data sets that can be applied to various stages of a project development.

Advances in Solar Heating and Cooling. http://dx.doi.org/10.1016/B978-0-08-100301-5.00002-3

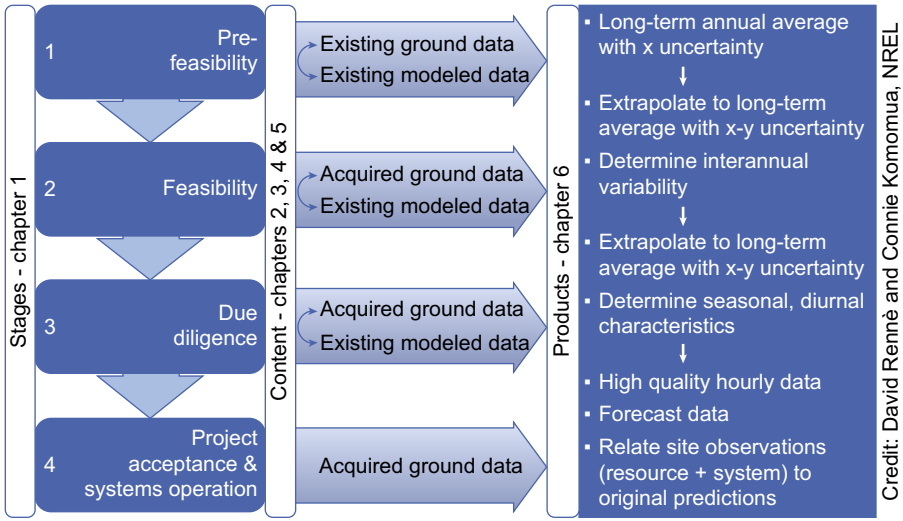

Figure 2.1 Four basic stages in a solar project development cycle, indicating basic resource data required for each cycle.
From Sengupta, M., Habte, A., Kurtz, S., Dobos, A., Wilbert, S., Lorenz, E., Stoffel, T., Renné, D., Myers, D., Wilcox, S., Blanc, P., Perez, R., February 2015. Best Practices Handbook for the Collection and Use of Solar Resource Data for Solar Energy Applications. Technical Report NREL/TP-5D00-63112. National Renewable Energy Laboratory, Golden, Colorado (USA).

The International Energy Agency's Solar Heating and Cooling Implementing Agreement has supported several solar resource assessment tasks since the program's beginning in 1977. Most recently, Task 36, "Solar Resource Knowledge Management," and Task 46, "Solar Resource Assessment and Forecasting," have brought together nearly 70 solar resource assessment experts from around the world to conduct benchmarking studies of solar resource data (measured and derived) and develop best practices in the development and use of solar resource data. Some of the information reported in this chapter has been developed through this international collaboration; further results can be found at http://task46.iea-shc.org.

2.2 Definition of solar resources

The solar radiation (or irradiance) at the top of the earth's atmosphere is called *extraterrestrial radiation* and the current accepted value for this "solar constant" (now referred to as the *total sky irradiance*) is 1366 W/m^2. The energy emitted by the sun is virtually invariant, estimated to be about 0.1% owing primarily to variations associated with sunspot cycles. Because of the eccentricity of the earth's orbit, however, the solar constant varies by about 6.7% throughout the course of a year (Vignola et al., 2012a).

The following terms related to solar resources are often found in the literature, and therefore a definition of each term is provided here:

Solar radiation: This term is often used interchangeably with *solar energy* and *irradiation* and, less commonly, *insolation*.

Radiant energy, or **radiance**: For the purposes of this chapter, this is the amount of energy emanating from the sun, and is generally expressed in units of W/m^2 sr. The sun radiates almost as a black body, at an effective temperature of 5778 K. Radiant energy (sometimes referred to as *radiant intensity*) decreases at the rate of the inverse square of the distance from the source.

Irradiance: This is the power density of radiation incident on a surface, or the rate at which radiant energy is incident on a surface, generally expressed in units of W/m^2.

Irradiation (or **insolation**): This is the quantity of solar energy (radiation) arriving at a surface during a specified period of time, generally expressed in units of W/m^2 h or W/m^2 year, or occasionally in MJ/m^2. Thus solar energy is synonymous with solar irradiation and also represents the *solar resource* available at a location over a specified time period.

The sun emits radiation across a broad spectrum of wavelengths, as shown in Fig. 2.2, in which the dashed line shows the spectral distribution of radiant energy reaching the top of the earth's atmosphere. The portion of the solar spectrum that is visible to the human eye is generally in the range of 380−780 nm, which is also the range in which the radiance emitted by the sun is at a maximum (the absolute

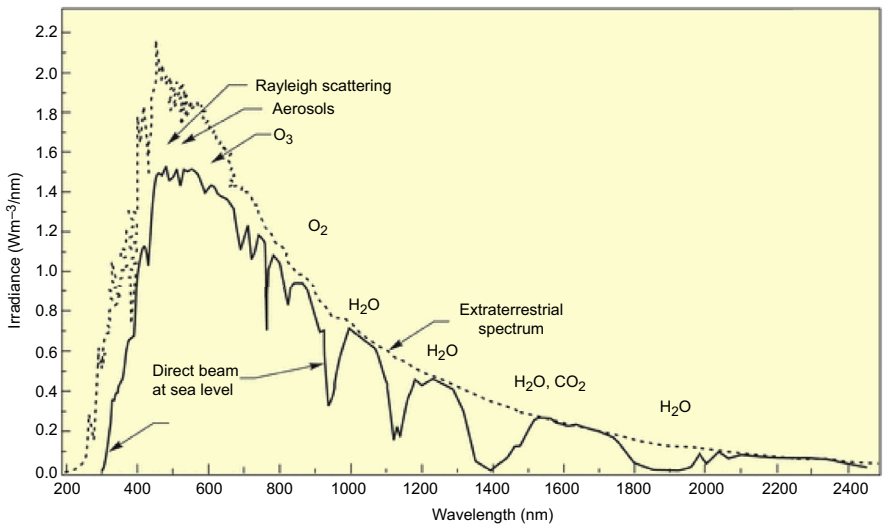

Figure 2.2 The spectral distribution of solar radiation reaching the top of the earth's atmosphere *(dashed line)* and at sea level *(solid line)*.
Image from StellarNet, Inc., http://www.stellarnet.us/popularconfigurations_radiosystems_solar.htm. See also Wehrli C. Extraterrestrial solar spectrum. Publication no. 615, Davos Dorf, Switzerland: Physikalisch-Meteorologisches Observatorium Davos, World Radiation Center, (PMOD/WRC); 1985 for further information on the solar spectrum at the top of the atmosphere.

maximum is at around 500 nm). This portion of the spectrum is called the *visible spectrum*. Radiation in wavelengths shorter than 380 nm is known as *ultraviolet* radiation, and radiation occurring in wavelengths longer than around 780 nm is called *infrared* radiation. The majority of solar radiation reaching the top of the earth's atmosphere falls in the spectral range of 300−3000 nm.

A variety of the molecular components of the atmosphere serve to absorb and scatter the incoming solar radiation at a number of discrete wavelengths, so that the spectral distribution of the radiant flux reaching the earth's surface can look quite different from the distribution at the top of the atmosphere, as shown in the solid line in Fig. 2.2. For example, Rayleigh scattering, aerosols, and ozone have a strong effect on reducing solar irradiance in the visible wavelengths at the earth's surface. Atmospheric dust and water droplets also serve to scatter radiation back to outer space. The reason the sky appears blue to the human eye is due to the preferential scattering of air molecules in the blue wavelength region of the visible spectrum (roughly 400−500 nm). Atmospheric water vapor absorbs solar energy in a number of wavelengths, especially in the infrared regions. Other trace gases in the atmosphere, such as CO_2 and methane, can also absorb solar radiation in a variety of spectral ranges (most notably in the infrared region), causing the temperature of the atmosphere to increase. The injection of additional CO_2 and methane into the atmosphere due to human activities is the well-known greenhouse gas effect, which can cause additional warming of the atmosphere due to these anthropogenic sources.

The definitions of the various *components* of the solar resource are also important. These are described in Fig. 2.3. The definitions apply primarily to the amount of radiation reaching the earth's surface in the visible spectrum.

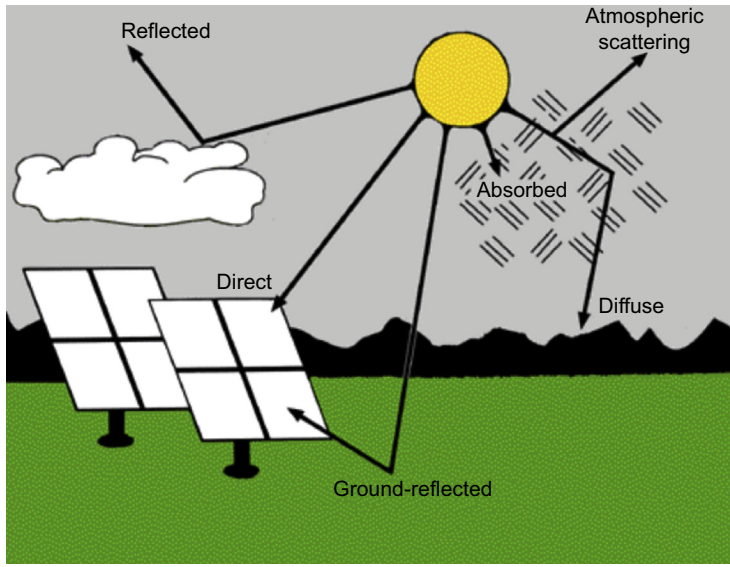

Figure 2.3 The components of the solar resource.
Image provided by NREL, courtesy of Tom Stoffel.

The amount of solar radiation from the sun reaching a flat surface at the earth's surface oriented normally to the sun's position throughout the day is known as *direct normal irradiance*, or DNI. As noted above, portions of the visible radiation reaching the top of the atmosphere can be scattered back to space or reflected toward the earth's surface by the presence of cloud droplets and aerosols. In addition, air molecules can absorb some of the radiation in the visible channels. Thus the total radiation reaching the earth's surface will be some combination of DNI and the radiation scattered back to the surface by cloud droplets and aerosols. The portion that is reflected by clouds and atmospheric aerosols is known as diffuse radiation. Measuring this component on a flat surface oriented horizontally gives the *diffuse horizontal irradiance*, or DHI. If we were to measure the total radiation falling on a flat surface horizontal to the earth's surface, we would be measuring both the solar radiation coming directly from the sun (assuming it is not obscured by a cloud) and the diffuse radiation from the clouds and sky. This, then, is the *global horizontal irradiance*, or GHI.

Thus GHI represents the total energy available from the sun and the sky on a horizontal surface and is usually the most important factor for understanding the resource available to flat plate collectors. DNI, on the other hand, is the most important component of solar radiation for understanding the energy that can be produced by concentrating collectors, such as curved mirrors used in trough technologies. Mathematically, the relationship between GHI and the other two components, DHI and DNI, is given as

$$\mathrm{GHI} = \mathrm{DNI} \times \mathrm{Cos}(Z) + \mathrm{DHI} \qquad [2.1]$$

where Z is the *solar zenith angle*, or the angle between the sun's position at any given time and the zenith, or a vertical line perpendicular to the earth's surface.

In most practical applications, flat plate collectors are generally oriented more directly toward the sun rather than on a horizontal plane. This is because a collector oriented more toward the sun will receive a higher global irradiance flux than flat surfaces for virtually all situations except for when the sun is directly overhead (at the zenith). Often, fixed flat plate collectors are oriented at an angle toward the south (in the Northern Hemisphere) equal to the latitude where the collector is installed. This is known as *latitude tilt*. In some cases flat plate collectors might even be mounted on one-axis or two-axis trackers to allow the collector to be oriented normal to the sun throughout the day and throughout the changing seasons. Even concentrating collectors will not always be oriented directly to the solar disk at all times, unless they are designed to track the sun throughout the day and throughout the seasons (two-axis tracking); in cases in which the concentrating collectors are not oriented directly toward the solar disk the direct irradiance flux will also be less than optimum.

2.3 Relationship between solar resources and solar collectors

Calculating global or diffuse radiation on a horizontal surface is useful as a global standard for being able to compare one site against another, regardless of the latitude or the

solar position with respect to the zenith; however, in virtually all circumstances the total radiation falling on a flat plate collector will be highest when the collector is oriented normal to the solar disk at any given time. Therefore, it is necessary to be able to convert the GHI or DNI values to the values received by a tilted surface to depict the solar resource available to the collector at any given time. The conversion of GHI to the irradiance received on a tilted surface is called *global tilt irradiance* (GTI). Fig. 2.4(a)–(c) provides schematic depictions of a fixed collector at latitude tilt and of one-axis and two-axis flat plate collectors.

As noted in Sengupta et al. (2015), a number of models are available to convert GHI or a combination of GHI and DNI into GTI, such as Temps and Coulson (1977), Hay (1979), Kluchar (1979), Liu and Jordan (1961), Reindl et al. (1990), and Gueymard and Myers (2008). For example, the following is a description of a simple method used to convert monthly and annual average GHI to GTI for one- or two-axis trackers as part of the products developed from the US National Solar Radiation Database (NSRDB), 1961–1990, as presented by Marion and Wilcox (1994).

The irradiance I_c reaching the surface of any of these types of collectors at any given time can be estimated from the following relationship:

$$I_c = I_b \mathrm{Cos}(\theta) + I_d + I_r \qquad [2.2]$$

where I_b is the incident direct beam radiation, I_d is the diffuse sky radiation, I_r is the radiation reflected from the earth's surface in front of the collector, and θ is the incident angle of the sun's rays to the collector. Algorithms developed by Menicucci and Fernandez (1988) were used for the US 1961–1990 NSRDB. The direct beam contribution, $I_b\mathrm{Cos}(\theta)$, was determined for each hour based on the DNI values reported in the NSRDB. The I_d was calculated from an anisotropic diffuse radiation model developed by Perez et al. (1990), based on DHI and DNI values from the NSRDB. The

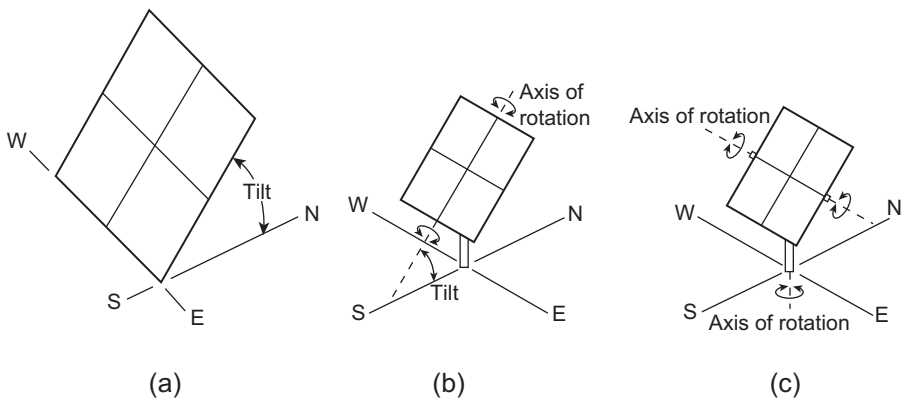

Figure 2.4 Three types of orientation options for flat plate collectors. (a) Facing south (in the Northern Hemisphere) at a fixed tilt; (b) one-axis tracking with axis of rotation oriented north–south; (c) two-axis tracking.

ground-reflected radiation received by the collector is determined from the GHI values in the NSRDB (I_h) along with the tilt of the collector from the horizontal (β) and the surface reflectivity or albedo (ρ), which is the fraction of the reflected to the incident radiation:

$$I_r = 0.5\rho I_h(1 - \cos\beta) \quad [2.3]$$

Values of surface albedo can generally be found in meteorological textbooks. Albedos for bright surfaces, such as surfaces covered by snow or light sand, are relatively high, and typically a value of 0.6 is chosen under these conditions. For surfaces covered with heavy vegetation an albedo of 0.25 is typically chosen.

For concentrating collectors there is very little (if any) contribution from the diffuse component or from ground reflection, so that the amount of radiation received by the collector, I_c, can be determined from the following:

$$I_c = \text{DNI} \times \text{Cos}(\theta) \quad [2.4]$$

However, particularly under hazy conditions, there could be a component of solar radiation coming from an enhanced bright aureole around the sun, called the *circumsolar radiation*. Although the circumsolar component may be factored into the DNI values based on the measurement or modeling approaches employed, the physical design of the solar collector may not be able to take advantage of this component. A detailed discussion of the extent to which the circumsolar component is captured in solar data, and the extent to which it affects a solar collector, can be found in Blanc et al. (2014).

2.4 Measuring and modeling the solar resource

For all solar thermal applications there are two primary means of obtaining solar resource data at a given location: (1) direct measurement of the solar resource using qualified instrumentation and accepted measurement practices and (2) modeling of the solar resource using "indirect" means, such as imagery of cloud characteristics observed from weather satellites, ground-based cloud cover observations, numerical weather prediction models, or sunshine duration records. This section provides an overview of best practices in measuring and modeling the solar resource for solar thermal applications.

2.4.1 Solar resource measurement techniques

Attempts to measure and quantify the amount of radiation arriving at the earth's surface from the sun date back to the early 1800s. An excellent historical perspective describing the evolution of solar measurement devices is provided in Vignola et al. (2012a). One of the earliest instruments, Pouillet's pyrheliometer (first built in 1837), was the first instrument to be called a *pyrheliometer* and was designed to

provide a first estimate of the *total sky irradiance*. In the early 1900s, development started on instruments that measured the total radiation from the sun and sky (the GHI), now referred to as *pyranometers.*

In the late 1800s, the Campbell−Stokes radiometer became a very popular instrument for determining the number of hours of direct solar radiation on a daily basis. This instrument functions by focusing the direct solar beam through a glass ball onto a strip of paper; when the sun is not obscured by a cloud, the focused beam burns a line on a strip of paper calibrated in a way that relates the length of the burn line to the length of time of direct sunlight. At the end of each day the total length of the burn mark is translated into the number of direct sunlight hours for the day. Although this approach provides only a crude depiction of the solar resource, the simplicity and ease of use of the instrument made it a popular component of weather stations throughout the world. Even today many of these instruments are still operational, particularly at airport weather stations in developing countries. However, empirical relationships must be developed to convert sunshine records to solar resource assessments, and generally very high uncertainties in the conversion can result. Thus it is not recommended to use these instruments for solar resource assessment purposes.

Another approach, using *bimetallic* sensors (eg, the Robitzsch bimetallic actinograph), was developed in the early 1930s and also came into very popular use at national weather stations throughout the world by the mid-century. These instruments can still be found in wide use today.

Around the beginning of the 20th century, efforts to develop instruments that convert the incoming solar radiation to an electrical output were undertaken, and today this is the most common approach for developing precise measurements of the solar resource. Today, these types of instruments fall into two broad categories: those using *thermopile*-type detectors and those using *silicon-diode*-type detectors. A thermopile detector works on the principle of the *thermoelectric effect*, whereby a voltage is generated from the temperature difference between two dissimilar metals. Today's precision pyranometers and pyrheliometers all make use of this effect by deploying two different metals under a glass dome (or double-glass dome) and monitoring the voltage output variations due to the passage of the sun across the sky and the obscuring of the sun by clouds and haze.

Silicon photodiodes are made from crystalline silicon that has been transformed into a semiconductor, similar to the principles of a crystalline−silicon PV cell. Instruments using this technology have the advantage of much lower cost and much faster response time than a thermopile-based instrument; however, they have significant disadvantages by being limited in their spectral response characteristics (they do not respond at all to wavelengths above 1100 nm) and are therefore subject to a slightly higher uncertainty than instruments using thermopile detectors.

Examples of thermopile-based pyranometers and pyrheliometers currently on the market are shown in Fig. 2.5(a) and (b), and an example of a silicon photodiode pyranometer currently on the market is shown in Fig. 2.5(c).

The use of thermopile radiometers became common beginning in the mid-1920s owing to the innovative work of companies such as Kipp & Zonen, and later, Eppley Laboratories and EKO Instruments, which continue to develop and refine improved

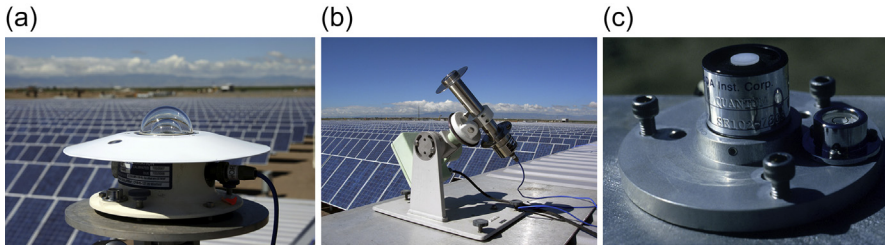

Figure 2.5 Examples of commercially available solar monitoring devices. (a) Eppley pyranometer, (b) Eppley pyrheliometer mounted on a tracker, and (c) LiCor silicon photodiode sensor.
Reproduced from NREL Image Gallery Nos. 15537, 15554, and 15483.

thermopile instruments for a variety of scientific purposes. Other companies such as Hukseflux and Yankee Environmental Systems have more recently entered thermopile-based products into the market. However, instruments based on silicon photodiode technology remain very common, because of their low cost, and can often be found in use at proposed and operational solar PV and solar thermal stations. In terms of accuracy and precision, the thermopile-type instruments and to a lesser extent the silicon photodiode−type instruments are currently the preferred choice for undertaking reliable solar resource measurement programs.

Solar resource measurement programs should be conducted in such a manner that the instrumentation used and the procedures followed in the measurement program follow globally accepted practices that ensure that the measurements can be clearly traced back to world reference standards. The globally accepted standard is the World Radiometric Reference (WRR), which is established every 5 years at the World Radiation Center in Davos, Switzerland, through an international pyrheliometer comparison (IPC). The IPC involves the use of a number of sophisticated thermopile-based precision instruments such as *absolute cavity radiometers*, operated by several global research institutions. The pyrheliometers used to establish the WRR can then be used in regional intercomparisons for purposes of identifying *reference radiometers*, which in turn can be used in the field as reference calibration sources for the instruments deployed at a given measurement site. In this way, the calibrations of the site-specific measurement can be traced back to the WRR through these intercomparison steps.

To obtain the most accurate complement of DNI, GHI, and DHI at a site, individual thermopile-based instruments must be used for each component; ie, a pyrheliometer on a tracking device for DNI and two pyranometers (one measuring GHI and one with the solar component blocked by a shading disk so that it measures only DHI). Because of the expense of such a configuration, there have been efforts under way to utilize a simpler, less costly but still reliable configuration, known as a *rotating shadowband radiometer*, or *RSR*.[1] The RSR basically consists of a silicon photodiode sensor

[1] In some cases, these instruments are referred to as Rotating Shadowband Pyranometers (RSPs) or Rotating Shadowband Irradiometers (RSIs).

Figure 2.6 Images of a rotating shadow-band radiometer (RSR). Left: Close-up of the shading arm passing over a silicon-diode sensor. Right: An RSR installed in the field. Reproduced from NREL Image Gallery Nos. 16994 (right) and 15484 (left).

mounted on top of a box that contains a motor and a shading band (see Fig. 2.6). The motor is designed to cause the shadow band to periodically pass over the field of view of the sensor. Because of the fast response time of the sensor, as soon as the shading band completely shades the sensor, the sensor is measuring only the DHI. At all other times the sensor is measuring the GHI. Based on these two measurements, the DNI can be calculated by solving Eq. [2.5] for DNI:

$$\mathrm{DNI} = (\mathrm{GHI} - \mathrm{DHI})/\mathrm{Cos}Z \qquad [2.5]$$

There has been extensive research undertaken to evaluate the uncertainties of thermopile-based pyrheliometers and pyranometers operated in the field, as well as the uncertainties in operational RSRs. For example, extensive comparative studies have been conducted at the National Renewable Energy Laboratory's (NREL's) Solar Radiation Research Laboratory in Golden, Colorado, and these studies have been published in Wilcox and Myers (2008), with an update published by Habte et al. (2014). A summary of uncertainty analyses for pyrheliometers and pyranometers is also provided in Sengupta et al. (2015). This report shows that pyrheliometers operated in the field following proper maintenance will have a subhourly uncertainty at the 95% confidence level of ±2%, whereas pyranometers will have an uncertainty of ±3% for solar zenith angles between 30° and 60°, and up to ±7−10% for solar zenith angles greater than 60°. The uncertainty of an RSR DNI measurement at the 95% confidence level is currently undergoing considerable research; in Vignola et al. (2012a) the uncertainty is reported at ±3.2%. Geuder et al. (2011), also reported in Sengupta et al. (2015), reported an uncertainty of about ±3% based on a study of 39 RSRs tested at Plataforma Solar Almería (PSA), Spain. Generally the uncertainties of an RSR are expected to be somewhat higher than with the thermopile instruments, although from the perspective of field operations these slightly higher uncertainties may be offset by their significantly lower costs. A 2015 study by Wilbert et al. (2014) provides a comprehensive overview of best practices for siting and operation of RSRs.

Other methods to develop a low-cost approach for measuring DNI are being tested and commercialized as of this writing. One such instrument is the SPN1, produced by Delta-T Devices (Fig. 2.7), which is capable of providing DNI, DHI, and GHI without the use of any moving parts. As described in Sengupta et al. (2015) this instrument consists of an array of seven thermopile detectors distributed under a glass dome in a hexagonal pattern. The sensors are located underneath a series of diffusers and a shadow mask, which is designed in such a way that throughout the day there will always be one or more detectors that are fully shaded from the sun and exposed to approximately half of the diffuse solar radiation (under overcast skies). In addition, one or more detectors are exposed to the full solar beam for all solar positions. The minimum and maximum readings of the seven detectors are then used to calculate GHI and DHI. Although at present the uncertainties of the outputs of this instrument are somewhat higher than those of the thermopile instruments or even the RSRs, based on testing at NREL and at PSA, work continues to improve the accuracy of this instrument, which can offer measurements of all three of the solar components at substantially reduced costs over the traditional suite of thermopile instruments.

2.4.2 Solar resource estimates using satellite data retrievals

In the early 1980s, when *geostationary weather satellites* (weather observation satellites that orbit at the same speed as the earth's rotation, so that they are always positioned 40,000 km above the equator at a fixed longitude) came into common use, efforts began to use the visible channel of the satellite to develop an estimate of the solar insolation at the earth's surface. Because of their fixed location above the earth's surface, these

Figure 2.7 The SPN1 pyranometer produced by Delta-T Devices.
Image provided by Delta-T, UK.

satellites have the advantage of being able to monitor cloud conditions almost continuously (every 15 min with modern-day geostationary satellites), at a visible channel resolution of about 1 km above the equator. However the "view" of these satellites is limited to the region between 60°N and 60°S. Furthermore, about five satellites spread around the world over the equator are necessary for obtaining a complete global view.

Weather services also make use of *polar-orbiting* satellites, which orbit the earth at low altitude (approx. 400 km) from pole to pole. Polar-orbiting satellites have the advantage of being able to observe the earth's clouds and surface at much higher resolution than geostationary satellites, owing to their much lower orbit, and of course, unlike geostationary satellites, they can cover the polar regions. However, because the earth is rotating under these satellites, a satellite generally passes over the same point on earth's surface just twice a day, making the time resolution of observing cloud patterns much coarser than with geostationary satellites.

Fig. 2.8 shows the current location of geostationary satellites around the world, operated by several countries. The figure also shows the typical coverage that is obtained from polar-orbiting satellites. The majority of the methods developed for solar resource assessment make use of geostationary satellite imagery, although the NASA Surface Meteorology and Solar Energy data set (https://eosweb.larc.nasa.gov/sse/) makes use of both geostationary and polar-orbiting satellites to obtain true global coverage.

The approaches developed to produce solar resource estimates from satellite observations can be categorized in three basic ways: *empirical methods*, whereby the strength of the visible signal at the satellite is correlated with various high-quality ground-based measurement stations; *semiempirical methods*, whereby the strength of the visible signal is compared with the ground albedo (as determined by monitoring

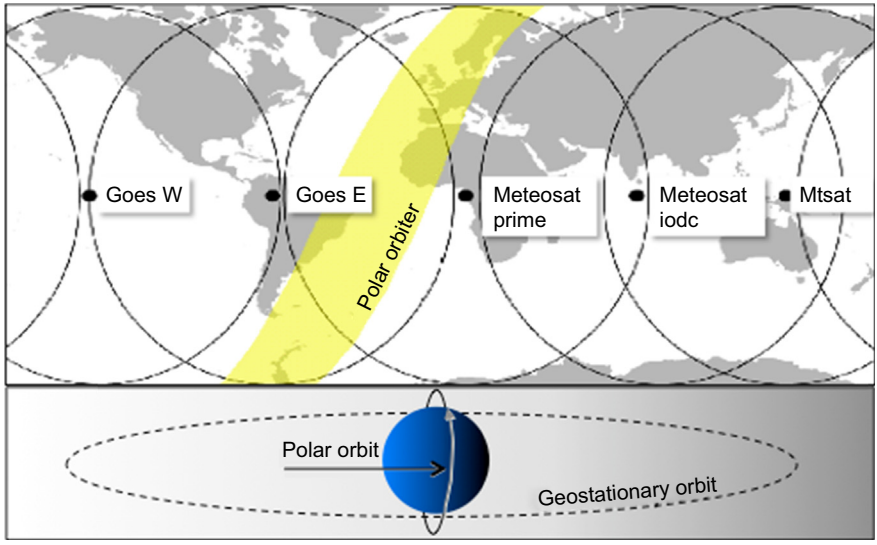

Figure 2.8 Current locations of modern-day geostationary satellites.
Image provided by Dr. Richard Perez, SUNY/Albany.

the signals at the satellite on clear days) to produce a "cloud index" from which a solar resource calculation can be made; and *physical methods*, whereby basic radiative transfer theory is applied to the satellite signals to develop a calculation of the solar irradiance at the earth's surface.

Today the semiempirical approach is the most common method used for solar resource assessments to support the solar industry, although data sets derived from both empirical methods and physical methods are also available.

One of the earliest approaches of the semiempirical method was the procedure developed by Cano et al. (1986). Many of the modern-day semiempirical approaches are based on Cano's original work. A version of this approach was developed a number of years ago by Dr. Richard Perez at the State University of New York, Albany (Perez et al., 2002) and is described below. This method has gone through a number of key improvements through the years, and currently the Perez model results are available as a SolarAnywhere product marketed by Clean Power Research. Other well-known products, such as the Heliosat Method, HelioClim, and the German Aerospace Institute's (DLR's) SOLEMI, or Solar Energy Mining product, as well as commercial products produced by companies such as GeoModel Solar and 3Tier, also have their roots from the Cano et al. approach. A summary of satellite-derived data sources can be found in Section 2.6.

The basic principles of the semiempirical approach, as reviewed by Renné et al. (1999) and illustrated in Fig. 2.9, depict the shortwave energy balance of the earth–atmosphere system.

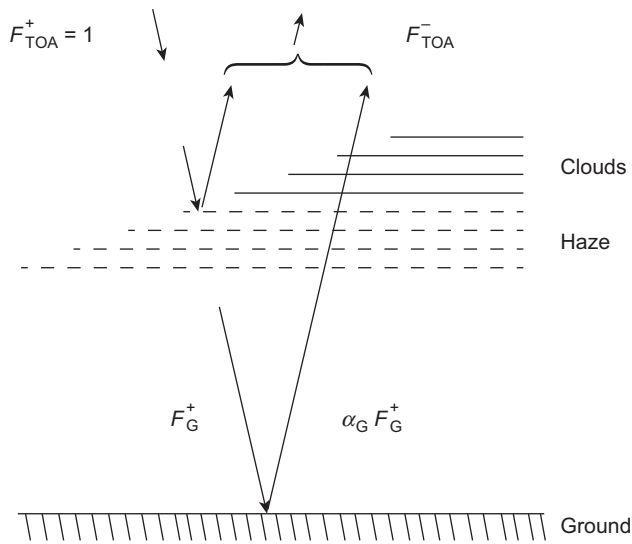

Figure 2.9 The shortwave energy balance of the earth–atmosphere system showing the relationship of the normalized incoming solar flux at the top of the atmosphere $\left(F^{+}_{TOA}\right)$, the reflected earth–atmospheric radiation measured by the satellite $\left(F^{-}_{TOA}\right)$, and the calculated ground irradiance $\left(F^{+}_{G}\right)$. α_G represents the albedo at the earth's surface.

In Fig. 2.9 we see that the net outgoing flux of shortwave radiation at the top of the atmosphere (TOA), or $F^{+}_{\mathrm{TOA}} - F^{-}_{\mathrm{TOA}}$ minus the amount absorbed by the atmosphere, F_{A}, is equal to the net flux at the surface, $F^{+}_{\mathrm{G}} - F^{-}_{\mathrm{G}}$ or $\alpha_{\mathrm{G}} F^{+}_{\mathrm{G}}$:

$$F^{+}_{\mathrm{TOA}} - F^{-}_{\mathrm{TOA}} = F^{+}_{\mathrm{G}}(1 - \alpha_{\mathrm{G}}) + F_{\mathrm{A}} \qquad [2.6]$$

Equation [2.6] forms the basis of the empirical–physical as well as the physical method, in which the effort is to solve the equation for F^{+}_{G}. The main differences among the various methods are the way in which the cloud cover is characterized by the satellite's measurement of F^{-}_{TOA} and how the forward- and backscattering due to atmospheric particles and the absorption of solar radiation by the various trace gases in the atmosphere, such as ozone and water vapor, is addressed.

For example, under clear sky conditions an accurate determination of the radiative transfer through the atmosphere that accounts for the absorption as well as the forward- and backscattering of the shortwave flux due to haze and trace gases is required. A number of clear sky radiative transfer models have been developed since 1995 to address this fundamental issue. Gueymard (2012) provides a comprehensive review of 18 clear sky models and determines that among the most reliable is the REST2. Another model in common use is the simplified broadband version of the SOLIS clear sky model, first published by Ineichen (2008). An overview of many clear sky models can also be found in Sengupta et al. (2015).

When clouds are present the visible channel of the satellite gathering data on the earth's shortwave reflectance at the top of the atmosphere is used. Modern-day weather satellites measure this value through a relative scale based on digital counts of the reflected radiation; the higher the counts, the higher the reflectivity of the earth–atmosphere system and, therefore, the higher the cloud cover. For example the Perez et al. (2002) method has introduced the concept of the cloud index, or C_i, which is determined at the satellite level by monitoring the irradiance measured by the satellite for 15–30 days until a "clear sky" albedo at the top of the atmosphere is determined; this then represents a C_i of 0. The higher the value of the irradiance reflected from the earth–atmosphere system, the higher the C_i, ie, $C_i = f\left(F^{-}_{\mathrm{TOA}}\right)$. In the case of the empirical–physical models, such as that of Perez et al. (2002), the C_i is expressed as follows:

$$F^{+}_{\mathrm{G}} / F^{+}_{\mathrm{G\text{-}Clear}} = 1 - \alpha_{\mathrm{TOA}} C_i \qquad [2.7]$$

Determination of C_i involves establishing a "dynamic range" of pixel counts received by the satellite for any given situation compared to the values determined at the lowest pixel count, which is assumed to be the clear sky value, $F_{\mathrm{G\text{-}Clear}}$ (under which $C_i = 1$). These conditions represent the maximum dynamic range possible for determining the C_i; ie, the difference between the lowest (darkest) pixel counts observed by the satellite (lowest F^{-}_{TOA}, or clear sky conditions) and the highest pixel counts that occur for F^{-}_{TOA}, which generally occurs under completely overcast conditions. When the dynamic range is at its highest level ($C_i = 1$) clear skies are assumed to

prevail ($F_{G}^{+} = F_{G\text{-Clear}}^{+}$ in Eq. [2.7]). Under these conditions, only the clear sky model chosen for the satellite method comes into play. As the dynamic range becomes smaller and smaller (in other words, as cloudiness increases), the C_i decreases until $C_i = 0$, in which case it is assumed that complete overcast conditions prevail, and other models in addition to the clear sky model also come into play.

A number of factors must be addressed to improve the accuracy of this very basic approach. One is the choice of the clear sky model and its features used in the methodology. Different clear sky models invoke somewhat different approaches in addressing Rayleigh and Mie scattering, especially in the way they handle the atmospheric *aerosol optical depth*, or AOD, which is a normalized measure of the amount of dust and haze particles in the atmosphere compared to a totally clean, dust-free atmosphere. Obtaining accurate data on the AOD is quite challenging, because there are very few routine global measurements of this parameter, and the way the various models address this critical influence of the transfer of solar radiation through the atmosphere represents one of the biggest differences among the various empirical–physical and physical approaches, especially with respect to the accuracy of the DNI calculations.

The various ways in which the individual DNI, GHI, and DHI components are calculated using these satellite approaches is also important. Even under totally overcast skies, although DNI is virtually zero, there is some GHI (due to the DHI produced by forward-scattering by the clouds), so it is important that the models handle the DHI component properly, using either empirical relationships or physical radiative transfer theory.

A third important factor in the empirical–physical approach is accurately determining the ground albedo. As noted earlier the low end of the dynamic range is established by a determination of the lowest amount of reflection from the earth–atmosphere system. However, the presence of snow cover, persistent low clouds or valley fog, or the reflection from bright sand or water surfaces can result in an erroneous selection of the lower threshold of the dynamic range. Thus it is necessary to develop independent data sources to ensure when high reflective values are due to snow, fog, or bright surfaces, rather than clouds. Some of the empirical–physical models make use of the infrared channels of the satellite to obtain a clearer understanding of ground conditions as well as certain cloud characteristics.

Another important factor under research is the impact that deep, vertical clouds might have on the calculations. The three-dimensional characteristics of clouds can be determined by using the infrared channels of the satellite, because cloud temperatures can be determined using these channels. Once cloud temperatures are known, their vertical extent in the atmosphere can be determined. However, factoring in the three-dimensional characteristics of the clouds as part of a satellite retrieval method for solar resource estimates can involve time-consuming physical radiative transfer theory, so methods for a fast radiative transfer scheme also need to be developed to take advantage of this additional information on cloud characteristics. Work is currently under way at NREL, with assistance from the University of Wisconsin and Colorado State University, to address a more physical-based approach to determining surface solar radiation (Sengupta et al., 2015).

In summary, satellite-derived estimates of the solar resource are now in common use. They have the capability of providing monthly accuracies as good as 5% for GHI and 10% for DNI, and these accuracies continue to improve with new developments. Satellite estimates also give us the capability of developing solar resource information at a very high spatial resolution (1 km^2 is possible) and an acceptable temporal resolution (15 min with modern-day satellites).

Section 2.6 summarizes a variety of satellite-based data sets available through public institutions and commercial vendors.

2.4.3 Other solar resource estimation techniques

Here we briefly describe other methods that have been developed or are being researched to provide reliable estimates of the solar resource at the earth's surface. Among the very first of these methods was the Angstrom relationship, a method developed in the early 1920s to convert sunshine records such as those obtained from Campbell−Stokes radiometers to actual solar resource estimates on a monthly basis. The method involved the creation of an empirical relationship established by relating the measurements from calibrated radiometers, such as thermopile instruments, to the sunshine records obtained from the more ubiquitous Campbell−Stokes radiometer. In its simplest form the Angstrom relationship can be written as

$$Q_G/Q_{TOA} = a + b(N/N_0) \quad [2.8]$$

where Q_G is the monthly mean global solar radiation at the earth's surface, Q_{TOA} is the monthly mean global radiation at the top of the atmosphere, N is the total observed number of monthly sunshine hours, N_0 is the monthly total possible duration of sunshine hours, and a and b are empirical coefficients that are a function of climate and geographic factors such as latitude, albedo, etc. This approach underwent a number of refinements through the years. We mention this approach here because it is referenced widely in the literature when reporting on country or regional solar resource assessments. However, satellite imagery offers a much more accurate and complete (spatial and temporal) estimate of the solar resource, and the use of solar resource information using a form of Eq. [2.8] is not recommended when reliable satellite estimates are available.

Another method involves converting cloud cover information obtained at national weather stations throughout the world into solar resource estimates using a variety of schemes involving clear sky models and empirical relationships based on the amount of cloud cover. When NREL developed the 1961−1990 NSRDB this approach was used extensively. The actual solar monitoring network using calibrated radiometers is quite limited in the United States (as in most countries), so to develop a comprehensive database for the country, it was necessary to resort to the use of cloud cover observations, which are available at virtually every weather station in the country. A model called METSTAT (described by Maxwell, 1998) was developed to convert the hourly cloud observations into hourly DNI, GHI, and DHI values at each station. Initially the database could be developed for only 239 weather stations throughout the

country. However, modifications to the original approach and the application of satellite-derived estimates made it possible to derive solar resource data for 1454 stations in the NSRDB update of 1991−2005. As the reliability of satellite estimates continues to improve, and demands increase for the finer spatial resolution possible with satellite-derived data, future national databases such as the NSRDB will rely more and more on satellite methods, with very little need for the ground-based data except for access to other ancillary weather information and to maintain a long-term data record from these stations.

A third approach receiving considerable attention is to develop solar resource estimates from numerical weather prediction (NWP) models. These models allow us to simulate atmospheric processes in great detail and to predict future atmospheric conditions out to as much as 2 weeks or more. As more and more solar technologies are installed in national electricity systems, solar resource forecasting is increasing in importance, and accurate ways of converting cloud information developed in NWPs into solar irradiance values are needed. Traditionally, NWPs have not been very accurate in predicting specific cloud types and cloud amounts, so there is currently an active amount of research under way to improve NWPs to predict solar resources with acceptable accuracy for operational purposes. Such a discussion of these methods is beyond the scope of this chapter, however.

2.5 Solar resource data sets important to siting and sizing solar heating and cooling (SHC) technologies

2.5.1 Resource variability—spatial

Owing to the temporal and spatial variability of the solar resource, it is important to have reliable site-specific information on the resource to properly size a solar system, whether it is a thermal or a PV system. The importance of this information increases as system sizes become larger and larger, because there are critical financial implications and risk factors associated with the use of data that have high or unknown uncertainty for siting and sizing a project.

The annual spatial variability of the GHI resource is relatively low, because the diffuse component of the incoming resource can partially offset the loss of the direct component when clouds pass across the sun. In the United States, for example, based on the most recent NSRDB updates as of this writing, the annual GHI resource varies by a factor of 2 across the country, ranging from under 1200 kWh/m^2 in the cloudier regions to approximately 2400 kWh/m^2 in the sunny desert southwest. Thus in general it is possible to make use of flat plate solar collectors virtually everywhere in the United States to meet local demands; what is important is understanding the local resource in sufficient detail to size and design the system properly.

The spatial variability of the DNI resource, however, can be quite high, and for concentrating collectors it is critical to understand the resource characteristics not only for proper sizing, but also even for siting of these systems, because their output

and economic feasibility will be highly dependent on the local resource. Using the United States as an example, the annual DNI resource varies by at least a factor of 3 (from around 2700 kWh/m^2 annually in the sunniest regions to about 900 kWh/m^2 in the cloudiest regions), and in addition shows much greater variability than GHI within certain regions. The value of DNI can be greatly influenced by local terrain and other effects on cloud formation.

Procedures for the optimal siting of solar systems generally involve the incorporation of spatial resource data, such as that derived from satellite methods, into Geographic Information Systems (GIS) software packages. This approach is preferred because other geospatial data, such as land use and landform features, transmission lines, highways and railways, ports, energy production facilities, load centers, protected areas, and areas excluded from development, can all be incorporated into the same software system to allow for overlaying of data sets to identify optimal sites. By establishing allowable thresholds of resource levels and then excluding all sites in these threshold regions where development cannot occur (such as protected areas), or where development might be optimal (such as proximity to load centers), the best sites for solar project development can be identified. Energy planners and government agencies use this approach to establish the technical resource potential of solar technologies and to determine optimum zones for development. This siting approach is best suited to large-scale systems requiring an ample resource, such as Concentrating Solar Power (CSP) systems, where a threshold value of, say, 5.5 kW/h day (2000 kW/h year) is established and then land use factors are taken into consideration to screen out all sites not suitable for development. An example of a regional site screening approach for CSP plants in the southwestern United States can be found in Section 6.1.2 of Sengupta et al. (2015).

2.5.2 Resource variability—temporal

The short-term temporal characteristics of the solar resource can have important effects on systems that respond immediately to irradiance fluctuations, such as PV systems. For these systems, when a cloud passes across the sun, casting a shadow on the system, a "ramp" in the solar resource occurs that results in a sudden drop in PV system output. Thus, for PV systems that have no internal built-in storage capabilities, understanding these "ramp rates" that can occur in time frames of seconds to hours is very important. However, systems that have built-in thermal storage, such as are typical of solar heating systems and now in large-scale CSP systems, are less affected by these short-term fluctuations or ramps.

The characteristics of longer-term variability, such as seasonal or interannual, are important for determining how systems might perform over the long run, whether or not they have storage capabilities. This is because most storage technologies serve only to mitigate short-term (subhourly) fluctuations and not those fluctuations that occur from day to day or season to season. Understanding interannual variability can also be important for determining a cash flow analysis of solar systems, although the interannual variability of the annual DNI resource is generally less than 10% and less than 5% for GHI.

2.5.3 Typical meteorological year data sets

Typical meteorological year (TMY) data sets represent 1 year of hourly (8760) weather data values extracted from long-term (at a minimum, 10 years) data records. TMY data sets are popular with building designers and others for modeling renewable energy systems, because they provide a relatively concise data set from which to develop system performance estimates. TMY data sets are generated by determining "typical" meteorological months from a process of weighting various weather parameters and then concatenating the months to form a typical year. TMY data sets do not provide information on extreme events and, by nature of the way they are created, do not necessarily represent actual conditions at any given time. Nevertheless they are useful for intercomparing system performance among different technology approaches without the need to ingest large amounts of data into simulation models.

There are various approaches for developing TMY data sets, but basically they are created from long-term weather records, which in many cases may require data filling. As described by Wilcox and Marion (2008), the TMY3[2] data set produced from the US NSRDB update is an empirical method that involves selecting 12 months of data from the 30-year record available in the NSRDB based on five weather parameters: GHI, DNI, dry bulb temperature, dew point temperature, and wind speed. An algorithm is created based on weighting factors applied to these five variables, so that individual months deemed "typical" of all 30 of those months would be selected, and then each month is concatenated with the next month without modification. The weighting factors assign priority to the solar radiation parameters, which means that the other weather parameters for a chosen typical month may not actually be typical.

Although TMY data sets remain in popular use today, with the convenience of being able to represent a long-term data set that may have missing data that required data filling measures, TMYs also have certain shortcomings that are important to understand, especially for financial institutions planning for the long-term cash flow expected from a project. The most important, of course, is that TMY data do not provide information on extreme events. The data incorporated into a TMY are essentially at the 50th percentile of the full distribution of possibilities; ie, the probability that a GHI value within a TMY will be exceeded is 50%. Thus a TMY data set is sometimes referred to as a P50 data set. If a developer is interested in learning what might happen to a system's performance during an unusually cloudy year, or a year in which there has been major volcanic activity causing partial obscuration of the solar resource, the TMY output will not be able to provide this information. Another important shortcoming of TMY data is that the 30-year data set from which it is derived is likely to have a number of "filled" data values, which otherwise would be missing owing to a

[2] In the United States, Sandia National Laboratories developed the original TMY data set in 1978. When NREL completed the NSRDB in the 1990s, a TMY data set was created out of this 30-year data set and designated as TMY2. An NSRDB update was produced that added in the years 1991−2005, and a new TMY data set was created, designated as TMY3, that makes use of the 1961−1990 data as well as the updated NSRDB data.

lack of observations during certain time periods, such as when a measurement device is down or a station is closed. Thus the TMY value may not represent the true long-term average value for a given parameter at a given site. Finally, as indicated in the next paragraph, the TMY data developed from the NSRDB are produced largely from modeled data sets based on the METSTAT model[3]; only about 2% of the data are actual measured data. Thus the TMY uncertainties include the uncertainties associated with the METSTAT model.

A good example of the difference between TMY data and long-term satellite-derived observations has been shown in a Clean Power Research white paper (2015). Fig. 2.10 compares TMY3 data for five local weather stations in and around the Minneapolis–St. Paul area of Minnesota in the United States with a commercial satellite-derived data set called SolarAnywhere, which is the commercial version of the Perez–SUNY/Albany model discussed in Section 2.4.2. The five stations have varying levels of data quality and completeness, resulting in differences in data quality and uncertainty across the stations. Stations indicated as class I have the lowest uncertainty, whereas class III stations have the highest uncertainty. The SolarAnywhere data cover the period 1998–2005, indicating that the TMY data are heavily weighted to solar resource estimates derived from a much earlier period than the satellite data. Fig. 2.10 shows that all of the five TMY3 stations differ from the satellite data on an annual basis, and in a few cases these differences are substantial, approaching 20%. Furthermore, the spatial pattern of the solar resource differs substantially for the two approaches, showing that spatial variability of GHI determined from the

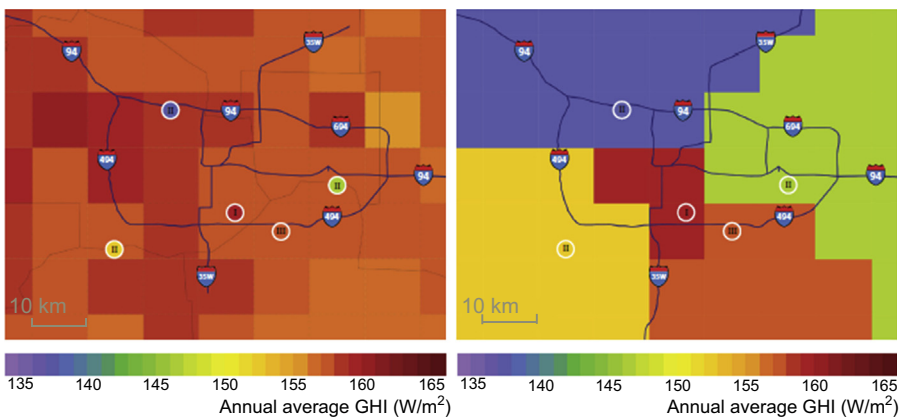

Figure 2.10 Comparison of TMY3 data with satellite-derived SolarAnywhere data for the Minneapolis–St. Paul region in the United States. The left panel shows the location of five TMY stations, including their uncertainty class (I is lowest, III is highest), with the 10-km satellite-derived data in the background. The right panel shows a gridded version of the TMY3 data based on a "nearest-neighbor" approach. It is evident from both panels that the TMY3 data can differ substantially in some cases from a more recent, validated, satellite-derived data set.

[3] Satellite data from 1998 to 2005 were used instead of the METSTAT model for the TMY3.

TMY3 stations is an unrealistically high 23 W/m^2 compared with 5 W/m^2 for the satellite-derived data. We present this information here to indicate to the reader the possible uncertainties that can result from the use of TMY data for making siting decisions and for designing and developing solar energy systems.

2.5.4 P50/P90 data sets

To avoid the concerns posed by TMY data project designers and developers and financial institutions financing these projects, data sets that provide information on *exceedance probabilities* of the solar resource should be used. For example, a P90[4] value represents the probability that a value will be exceeded 90% of the time. Exceedance values can be developed from a cumulative distribution function (CDF) of a parameter available from a large data set, such as the NSRDB. For example, Dobos et al. (2012) have looked at the NSRDB GHI and DNI data for Phoenix, Arizona, and produced CDF's of these data to illustrate the concept of P50 and P90 (Fig. 2.11). Fig. 2.11 shows that, if the annual Phoenix data were fit to a normal distribution (solid line), at CDF = 0.1 (the P90 value), an annual GHI of 2.2 MWh/m^2 will be exceeded 90% of the time (or conversely, the solar resource falls below this value 10% of the time). Similarly, for DNI, the hourly solar resource exceeds 1.96 MWh/m^2 90% of the time. However, long-term solar data do not necessarily follow a normalized distribution, so Fig. 2.11 also shows that the P90 value is somewhat lower in Phoenix when determined from an actual versus a normalized distribution.

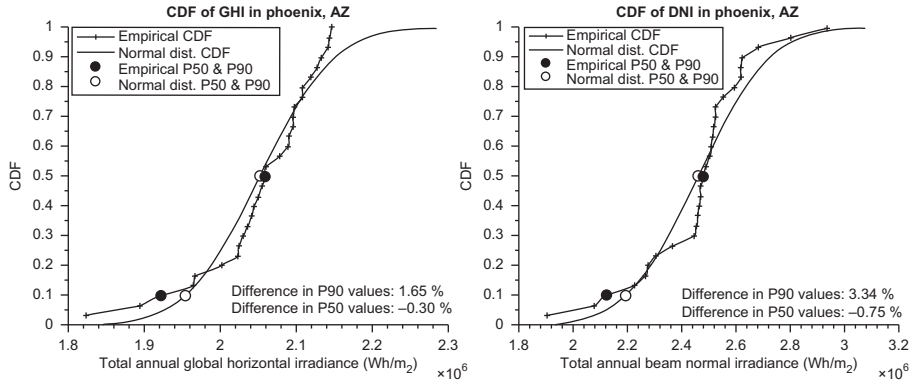

Figure 2.11 CDF of GHI (left) and DNI (right) for Phoenix, Arizona (USA) as determined from the 30-year NSRDB.
From Dobos, A., Gilman, P., Kasberg, M., 2012. P50/P90 analysis for solar energy systems using the systems analysis model. Conference Paper NREL/CP-6A20-54488, June 2012. National Renewable Energy Laboratory, Golden, Colorado. Presented at World Renewable Energy Congress, Denver, 2012.

[4] We use P90 here as an example. Other exceedance probabilities, such as P70 and P95, are also of interest to certain project designers and financial organizations.

2.5.5 The influence of data uncertainty on P90 values

A major motivation for developing exceedance probabilities for solar data sets (or for system performance parameters) is to give financial institutions information on the "bankability" of a project. Rather than just knowing what a system output might be under "typical" conditions, exceedance probabilities provide information on the amount of time a system is expected to exceed certain performance levels. For example, Dobos et al. (2012) show that if the P90 performance level of a system is 10,000 kWh-year^{-1} then this value would be exceeded in 90% of all of the years representing the total data set. Further discussion on data bankability can be found in Vignola et al. (2012b) and Gueymard (2014).

The effect of reducing the uncertainty of the true long-term solar resource at a site (which can be accomplished in a variety of ways) as a way of reducing financial risk is demonstrated in Fig. 2.12, taken from a study by Moody's Investors Services (2010). Fig. 2.12 shows that with only 1 year of data, the uncertainty of the value and the distribution of the true long-term mean is much higher than with 10 years of data. Thus, assuming that a long-term annual data set follows a Gaussian or normal distribution (which is not necessarily the case, as was shown in Fig. 2.11), the standard deviation that is assigned to a 1-year data set is much higher than for a 10-year data set, because there is more information associated with the 10-year data set. Although the median value of the distribution does not change between the 1-year and the 10-year distribution curves, the P90 value increases with the additional knowledge (lower uncertainty) associated with having a 10-year data set, which would lower the financial risk of the project.

2.5.6 Reducing uncertainty: site adaptation

As shown in Section 2.5.5, a bankable solar energy project relies on solar resource data with specified uncertainties from which investors can better understand the risk of times when performance of the system will be lower than desired. Reducing uncertainty in solar resource data is thus a key step toward producing bankable projects.

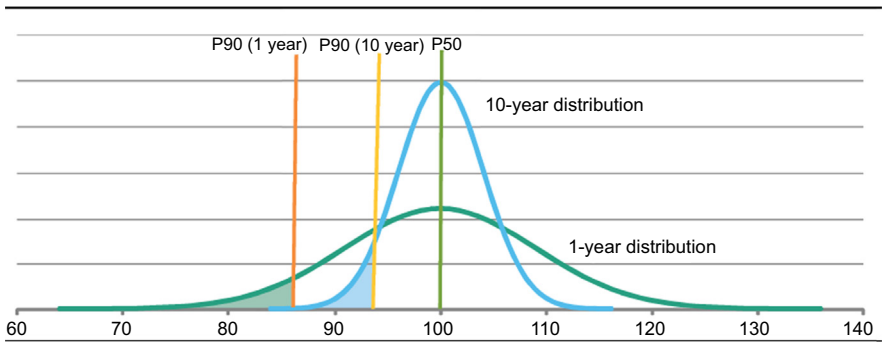

Figure 2.12 Example showing how reducing data uncertainty reduces financial risk by increasing P90 values.
From Moody's Investors Services, July 28, 2010. PV Solar Power Generation Projects. Special Comment.

There are several steps that can be taken to reduce data uncertainty and therefore project risk:

1. Collect high-quality on-site ground data for many years: this is the best way to provide the lowest risk data set to a financial organization; however, it is generally impractical owing to the time required to collect sufficient data (5−10 years);
2. Collect high-quality on-site ground data for a short time (1 year or less): this would be a more practical approach with respect to investor time scales, but, as indicated in Fig. 2.12, this poses higher risk to investors because they have limited knowledge of interannual variability and solar resource trends and therefore have high uncertainty as to whether the actual measurement period represents a high-resource or a low-resource annual value.
3. Obtain multiyear satellite-derived or other model-derived data sets: In the previous sections we have noted that we can use ancillary weather data, such as weather satellite imagery or ground observations of cloud cover, to produce long-term data sets when measurements are not available (which is the typical case). This is a relatively inexpensive way to capture enough data to produce P90 values; however, the risk to investors using these modeled data, with their inherently higher uncertainties, is higher than if actual high-quality measured data for the same time period were available.
4. Merge long-term modeled (eg, satellite-derived) data with short-term high-quality on-site measured data: this approach, known as *site adaptation*, is the most practical and cost-effective approach for developing reliable solar data for a project and offers the lowest risk to developers without causing lengthy project delays.

A detailed description of data adaptation methods is beyond the scope of this chapter; a 2015 publication by Polo et al. (2015) provides a comprehensive review of these methods. However, a few basic approaches are highlighted here. Perhaps the most straightforward approach is the *ratio method*. In this method, the ratios of selected periods of concurrent independent data sets (a short-term measurement data set concurrent with the long-term modeled data set) are calculated, and then the ratios are applied to the remaining long-term data set (Gueymard and Wilcox, 2009). However, the uncertainties in this approach increase if the biases in either data set vary from time to time. Furthermore, if there are long-term trends in the data the length of time required for the measured data set increases.

Another approach is to combine two independent data sets using weighting criteria (Meyer et al., 2008). The weighting can be determined based on data uncertainties, and additional data sets can even be included without compromising overall data uncertainty. Although this method was designed primarily for merging two different modeled data sets, measured data sets can also be included if their uncertainties are known.

A third approach is to use the CDF of ground-based data to improve satellite-derived data (Schumann et al., 2011). This approach reduces bias errors and improves Kolmogorov−Smirnov integrals (KSIs) in the satellite data. Mieslinger et al. (2014) have improved on this approach by determining both the systematic and the random deviations of the data sets based on mean bias (for systematic) and standard deviation (for random) statistics and using the KSIs to quantify the differences in the CDFs. Polynomial expressions are then used for the data adaptation. This approach is especially useful when there are large deviations between the satellite-derived and the ground-measured data. The approach requires at least 1 year of overlapping data, but preliminary results show that the corresponding biases approach zero.

2.6 Sources of solar resource information

This section provides a summary of publicly available sources of solar data, both measured and modeled, as well as key ongoing programs such as the IRENA Global Atlas and the World Bank/ESMAP resource mapping program.

Sengupta et al. (2015) provide a comprehensive summary of historical and current sources of data and data products available both through the public domain and through private companies (see Chapter 5.4 of this NREL study). Table 2.1 provides a summary of selected data sets available as of this writing, encompassing both measured and modeled data sources, derived from the NREL report.

A key development over the past few years has been the production of the International Renewable Energy Agency's (IRENA's) Global Atlas for Renewable Energy (gobalatlas.irena.org). The Atlas significantly extends an effort first started in 1999 known as the Solar and Wind Energy Resource Assessment (SWERA) project, funded by the Global Environment Facility and managed by the United Nations Environment Programme. SWERA ended in 2007, so with the formation of IRENA in 2010 the SWERA data, which resided initially with the UNEP/Global Resource Information Database in Sioux Falls, South Dakota (USA), and more recently at NREL (http://maps.nrel.gov/swera), are now incorporated into the Global Atlas. IRENA's Global Atlas provides basic foundational information on national renewable energy potentials to remove knowledge barriers and stimulate national renewable energy investments and policy formulation. The Global Atlas initially incorporated wind and solar data, but is now being expanded to include data for all renewable energy resources.

Another key development launched in October 2012 is the World Bank's Energy Sector Management Assistance Program (ESMAP) solar and wind resource mapping project (http://www.esmap.org/RE_Mapping). This project develops renewable energy resource mapping at the country level to support government planning and commercial development. The solar mapping activities include a combination of GIS-based mapping using satellite-derived techniques, with enhancements in some cases provided by NWP models. Countries that currently have very limited information on resource potential are targeted for this program, and projects are executed through the World Bank and supported by ESMAP with both funding and technical support. At the time of this writing preliminary high-resolution solar mapping has been completed for several countries (Pakistan, the Maldives, Malawi, Zambia, and Tanzania) and measurement programs have been initiated to validate the maps.

2.7 Summary

Although solar resource information has been available in a variety of formats for a number of years, the rapid growth in solar technology deployments, combined with improved ways of both measuring and modeling the solar resource, has resulted in significant activity at regional and national levels to improve and make more accessible the quality and completeness of these data. Furthermore, the many types of products

Table 2.1 Listing of selected available solar resource data sources

Name of data source	URL	Period of record	Coverage	Data elements
World Radiation Data Center (WRDC)	http://wrdc.mgo.rssi.ru	1964–present	Global (>1000 measurement stations)	Primarily daily total GHI; some DNI
European Solar Resource Atlas (ESRA)	http://www.soda-is.com/eng/index.html	1981–1990	Europe, 10-km resolution	Daily and monthly GHI, DHI, DNI
HelioClim (Ecole des Mines de Paris/Armines)	http://www.soda-is.com/eng/index.html	1985–present	Europe, Africa, Mediterranean Basin (5-km resolution)	Hourly, daily GHI
PVGIS (Joint Research Centre, Italy)	http://re.jrc.ec.europa.eu/pvgis/download/download.htm.	1981–1990	Europe, Mediterranean region, Africa, southeast Asia; nominally 30-km resolution	Monthly, annual GHI (Europe), daily GHI elsewhere
METEONORM 7.1.4 (Meteotest, Switzerland)	http://meteonorm.com	1991–2010	Global interpolated data from ~8325 stations	GHI, DHI, DNI, other
NASA Surface Meteorology and Solar Energy	https://eosweb.larc.nasa.gov/sse/)	July 1983–June 2005	Global, 100-km resolution	GHI, DHI, DNI
DLR-ISIS (German Aerospace Institute	http://www.pa.op.dlr.de/ISIS.	1984–2004	Global (280-km resolution)	DNI, GHI
Solar Data Warehouse	http://solardatawarehouse.com.	Up to 25 years to present	USA (~3000 measurement stations)	GHI

Continued

Table 2.1 Continued

Name of data source	URL	Period of record	Coverage	Data elements
US National Solar Radiation Data Base Updates	www.nsrdb.nrel.gov	1961–2010	USA (1454 stations, mostly modeled)	GHI, DHI, DNI, other
Baseline Surface Radiation Network	www.bsrn.awi.de/en/home/wrmc/.	1992–present	Global (~40 measurement stations)	GHI, DHI, DNI, other
3Tier by Vaisala	http://www.3tier.com/en/support/resource-maps/	1997–present	Global maps (commercial data sets available)	GHI, DNI
SolarAnywhere (Clean Power Research)	www.cleanpower.com/SolarAnywhere.	1998–present	North America (10-km, other commercial data sets available)	GHI, DHI, DNI
GeoModel Solar (Slovakia)	http://geomodel.eu/index.php	April 2004–present	Europe, Africa, and the Middle East (5-km resolution, available commercially)	GHI, DHI, DNI, other

Derived from From Sengupta, M., Habte, A., Kurtz, S., Dobos, A., Wilbert, S., Lorenz, E., Stoffel, T., Renné, D., Myers, D., Wilcox, S., Blanc, P., Perez, R., February 2015. Best Practices Handbook for the Collection and Use of Solar Resource Data for Solar Energy Applications. Technical Report NREL/TP-5D00-63112. National Renewable Energy Laboratory, Golden, Colorado (USA).

required by government policy makers, project developers, system operators, and financial institutions have been a very strong impetus to expand and improve on the type of information available. This chapter has provided a snapshot of best practices in collecting and using solar resource data for solar heating and cooling siting and performance applications. The reader is encouraged to go to the references and the URL links provided in the text to obtain more comprehensive information about solar resources and how solar resource data can be applied to all solar energy applications.

References

Blanc, P., Espinar, B., Geuder, N., Gueymard, C., Meyer, R., Pitz-Paal, R., Reinhardt, B., et al., 2014. Direct normal irradiance related definitions and applications: the circumsolar issue. Solar Energy 110, 561−577.

Cano, D., Monget, J.M., Albuisson, M., Guillard, H., Regas, N., Wald, L., 1986. A method for the determination of the global solar radiation from meteorological satellite data. Solar Energy 37 (1), 31−39.

Clean Power Research, 2015. How Misuse of Solar Resource Datasets Is Reducing Solar Industry Profits. White Paper, Clean Power Research, Kirkland, Washington.

Dobos, A., Gilman, P., Kasberg, M., 2012. P50/P90 analysis for solar energy systems using the systems analysis model. In: Conference Paper NREL/CP-6A20-54488, June 2012. National Renewable Energy Laboratory, Golden, Colorado. Presented at World Renewable Energy Congress, Denver, 2012.

Geuder, N., Hanussek, M., Halle, J., Affolter, R., Wilbert, S., 2011. Comparison of corrections and calibration procedures for rotating shadowband irradiance sensors. In: SolarPACES conference. Granada, Spain.

Gueymard, C.A., Myers, D., 2008. Validation and ranking methodologies for solar radiation models. In: Badescu, V. (Ed.), Modeling Solar Radiation at the Earth's Surface. Springer.

Gueymard, C.A., 2012. Clear-sky irradiance predictions for solar resource mapping and large-scale applications: Improved validation methodology and detailed performance analysis of 18 broadband radiative models. Solar Energy 86, 2145−2169.

Gueymard, C.A., 2014. A review of validation methodologies and statistical performance indicators for modeled solar radiation data: towards a better bankability of solar projects. Renewable and Sustainable Energy Reviews 39, 1024−1034.

Gueymard, C.A., Wilcox, S.M., 2009. Spatial and temporal variability in the solar resource: assessing the value of short-term measurements at potential solar power plant sites. In: Proceedings, Solar 2009. American Solar Energy Society Proceedings, Buffalo, New York.

Hay, J.E., 1979. Study of Shortwave Radiation on Non-Horizontal Surfaces. Report 79−12. Atmospheric Environment Service, Downsview, Ontario.

Habte, A., Wilcox, S., Stoffel, T., February 2014. Evaluation of Radiometers Deployed at the National Renewable Energy Laboratory's Solar Radiation Research Laboratory. Technical Report NREL/TP-5D00−60896. National Renewable Energy Laboratory, Golden, Colorado (USA).

Ineichen, P., 2008. A broadband simplified version of the SOLIS Clear-sky model. Solar Energy 82, 758−762.

Kluchar, T.M., 1979. Evaluation of models to predict insolation on tilted surfaces. Solar Energy 23, 111−114.

Liu, B.Y.H., Jordan, R.C., 1961. Daily insolation on surfaces tilted towards equator. ASHRAE Transactions 67, 526−541.

Marion, W., Wilcox, S., 1994. Solar Radiation Data Manual for Flat-Plate and Concentrating Collectors. NREL/TP-463−5607. National Renewable Energy Laboratory, Golden, CO.

Menicucci, D., Fernandez, J.P., 1988. User's Manual for PVFORM: a Photovoltaic System Simulation Program fro Stand-alone and Grid-Interactive Applications. SAND85-0376. Sandia National Laboratory, Albuquerque, New Mexico.

Maxwell, E.L., 1998. METSTAT − the solar radiation model used in the production of the national solar radiation data base (NSRDB). Solar Energy 62 (4), 263−279.

Moody's Investors Services, July 28, 2010. PV Solar Power Generation Projects. Special Comment.

Meyer, R., Torres Butron, J., Marquardt, G., Schwandt, M., Geuder, N., Hoyer-Klick, C., Lorenz, E., Hammer, A., Beyer, H.G., 2008. Combining solar irradiance measurements and various satellite-derived products to a site-specific best estimate. In: Proceedings, Solar-PACES Conference, March 4−7, 2008, Las Vegas, Nevada.

Mieslinger, T., Ament, F., Chhatbar, K., Meyer, R., 2014. A new method for fusion of measured and model-derived solar radiation time-series. Proceedings, SHC 2013: International Conference on Solar Heating and Cooling for Buildings and Industry, Energy Procedia 48, 1617−1626.

Perez, R., Ineichen, P., Seals, R., Michalsky, J., Stewart, R., 1990. Modeling daylight availability and irradiance components from direct and global irradiance. Solar Energy 44 (5), 271−289.

Perez, R., Ineichen, P., Moore, K., Kmiecik, M., Chain, C., George, R., Vignola, F., 2002. A new operational model for satellite-derived irradiances: description and validation. Solar Energy 73 (5), 307−317.

Polo, J., Wilbert, S., Ruiz-Arias, J.A., Meyer, R., Gueymard, C., Suri, M., Martín, L., Mieslinger, T., Blanc, P., Grant, I., Boland, J., Ineichen, P., Remund, J., Escobar, R., Troccoli, A., Sengupta, M., Nielsen, K.P., Renné, D., Geuder, N., 2015. Integration of Ground Measurements to Model-Derived Data. IEA-shc Task 46 Solar Resource Assessment and Forecasting. Final Report for Subtask B3. To be available at: http://task46.iea-shc.org/publications.

Reindl, D.T., et al., 1990. Evaluation of hourly tilted surface radiation models. Solar Energy 45, 9−17.

Renné, D.S., Perez, R., Zelenka, A., Whitlock, C., DiPasquale, R., 1999. Use of weather and climate research satellites for estimating solar resources (Chapter 5). In: Yogi Goswami, D., Böer, K.W. (Eds.), Advances in Solar Energy, vol. 13. American Solar Energy Society, Boulder, Colorado, 457 pp.

Sengupta, M., Habte, A., Kurtz, S., Dobos, A., Wilbert, S., Lorenz, E., Stoffel, T., Renné, D., Myers, D., Wilcox, S., Blanc, P., Perez, R., February 2015. Best Practices Handbook for the Collection and Use of Solar Resource Data for Solar Energy Applications. Technical Report NREL/TP-5D00-63112. National Renewable Energy Laboratory, Golden, Colorado (USA).

Schumann, K., Georg Beyer, H., Chhatbar, K., Meyer, R., 2011. Improving satellite-derived solar resource analysis with parallel ground-based measurements. In: Proceedings, Solar World Congress 2011. International Solar Energy Society, Kassel, Germany.

Temps, R.C., Coulson, K.L., 1977. Solar radiation incident up on slopes of different orientations. Solar Energy 19, 179−184.

Vignola, F., Joseph, M., Stoffel, T., 2012a. Solar and Infrared Radiation Measurements. CRC Press, Taylor & Francis Group, Boca Raton, Florida, 394 pp.

Vignola, F., Grover, C., Lemon, N., MacMahan, A., 2012b. Building a bankable solar radiation dataset. Solar Energy 86, 2218−2229.

Wehrli, C., 1985. Extraterrestrial Solar Spectrum. Publication no. 615. Physikalisch-Meteorologisches Observatorium Davos, World Radiation Center, (PMOD/WRC), Davos Dorf, Switzerland.

Wilcox, S., Myers, D., 2008. Evaluation of Radiometers in Full-Time Use at the National Renewable Energy Laboratory Solar Radiation Research Laboratory. NREL/TP-550−44627. National Renewable Energy Laboratory, Golden, CO.

Wilbert, S., Geuder, N., Schwandt, M., Kraas, B., Jessen, W., Meyer, R., Nouri, B., 2014. Best practices for solar irradiance measurements with rotating shadowband irradiometers. In: Prepared Within IEA Task 46 Subtask B1, and INS Project 1268. Available at: http://task46.iea-shc.org/publications.